５章　強震動観測による地殻及び基盤構造の調査

5.1

Rupture processes of the 2004 Chuetsu (mid-Niigata prefecture) earthquake, Japan: A quintuple shock in a complex fault system

Kazuhito Hikima and Kazuki Koketsu

Abstract

We first relocated the hypocenters of the events in the 2004 Chuetsu earthquake sequence, Niigata, Japan, using the double-difference method. The resultant distribution of aftershocks indicates a complex fault system consisting of five different fault planes. We then performed the inversions of strong motion records for the rupture processes of the five major events (quintuple shock). The results indicate that the mainshock ($M_{\rm W}$ 6.6) and the largest aftershock ($M_{\rm W}$ 6.3) occurred on parallel fault planes with a NNE-SSW strike and westward dip. The zones of large slips (asperities) are located near the hypocenters of the events. However, the other three events (M_W 5.9, 5.7 and 5.9) occurred on fault planes dipping eastward, which are perpendicular to that of the mainshock. We also estimated the Coulomb failure stress changes immediately before the major events using the slip distributions deduced from the waveform inversions. The obtained ΔCFFs were positive at the rupture breaks (hypocenters) and in the asperities of the major aftershocks. These results suggest that the stress change caused by preceding earthquakes led to a series of earthquakes in the complex fault system. The vital aftershock activities also resulted from this fault system.

1. Introduction

An earthquake with a JMA magnitude ($M_{\rm JMA}$) of 6.8 occurred in the Chuetsu region of the Niigata prefecture, central Japan at 17:56 on October 23, 2004 (JST=UT+9 hours) [*JMA*: Japan Meteorological Agency, 2005]. This mainshock was followed by vital aftershock activities, so that the number of large aftershocks was significantly greater than other crustal earthquakes in Japan. In particular, it is notable that four aftershocks with JMA magnitudes of 6.0 or greater occurred at 18:03 ($M_{\rm JMA}$ 6.3), 18:11 ($M_{\rm JMA}$ 6.0) and 18:34 ($M_{\rm JMA}$ 6.5; largest aftershock) on the same day, and at 10:40 on October 27 ($M_{\rm JMA}$ 6.1). The mainshock and these M6 aftershocks show the 2004 Chuetsu (mid-Niigata prefecture), Japan, earthquake sequence to be a quintuple shock in the same fault system (Figure 1).

Despite the moderate size of the earthquakes, their sequence resulted in serious disasters such as 46 people killed, 4,301 injured, and 2,827 houses destroyed [*FDMA*: Fire and Disaster Management Agency, 2005] including thousands of landslides [*Sidle et al.*, 2005]. In order to examine the cause of the singular earthquake sequence and seismic activities, *Kato et al.* [2005] elucidated

the velocity structure around the source region of the earthquakes. This study also pursues the cause by determining the accurate geometry of the source fault system. We will relocate the hypocenters of the major events and small aftershocks, and derive candidate fault planes from resultant aftershock distributions. We will then perform the inversions of strong motion records for the rupture processes of the major events. Since every event has two candidate planes, which are perpendicular to each other, we will carry out the inversions twice and choose the plane with a better fit. We will finally calculate static stress change using the deduced fault geometry and slip distributions, and discuss the interactions among the major events.

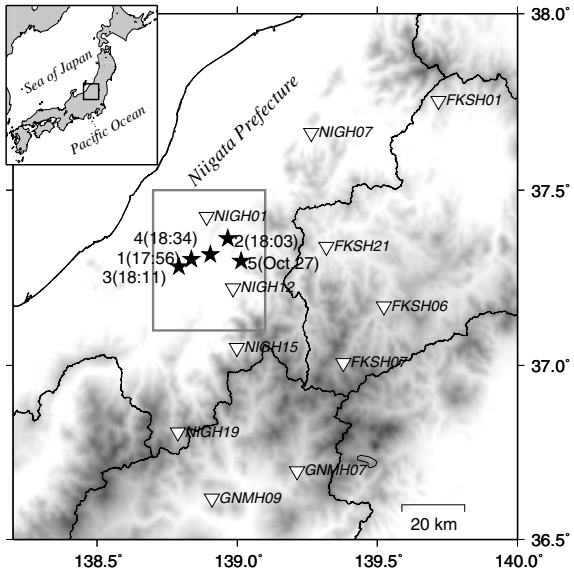

Fig. 1. Index map of the 2004 Chuetsu earthquake sequence. The rectangle drawn by thick lines is the target area of this study. The stars denote the epicenters of the five major events, and the numbers labeled them indicate the chronological order of occurrence. The reverse triangles represent the KiK-net stations observing the strong motion records studied.

2. Aftershock Distribution

As the classical theory that "aftershocks roughly define the fault plane of their mainshock" [e.g., *Page*, 1968] must be valid for the major events of the Chuetsu earthquake sequence, we need the accurate locations of aftershock hypocenters. Although the Seismological and Volcanological Bulletin of Japan [*JMA*, 2005] is one of the most reliable catalogs of hypocenter information in Japan, the locations in this bulletin include an obvious bias toward the southeast because of the high irregularity in the velocity structure around the source region [*Kato et al.*, 2005]. Accordingly, we re-determined the loci of the major events and small aftershocks using arrival times in the bulletin and the double-difference (DD) method [*Waldhauser and Ellsworth*, 2000].

The depth profile of the resultant aftershock distribution suggests five fault planes as shown in Figure 2. The mainshock (event 1) and largest aftershock (event 4) are located on the distinct

planes dipping westward, which are parallel to each other (planes A and D). The event 5 is also on the distinct plane E perpendicular to these planes connecting them. However, the fault planes of the other two events are not so obvious. The event 3 is close to the event 1, but it does not look to be on the plane A. It seems to be located on the vague plane C perpendicular to the plane A. We can also find the vague plane B to be a perpendicular plane connecting the planes A and D, and the event 2 to be located on this plane. Therefore, all the events should have had different fault planes, if rupture process inversions confirm that the events 2 and 3 occurred on the planes B and C, respectively.

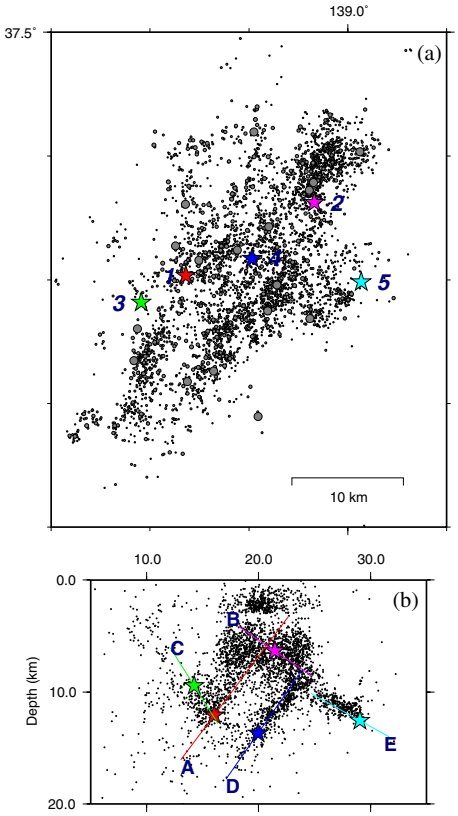

Fig. 2. Relocated epicenters of the major events (stars) and small aftershocks (upper) and their depth profile perpendicular to the mainshock strike (lower). The lines with capital letters in the depth profile represent the candidates of fault planes.

3. Rupture Process Inversions

For the rupture process inversions, we used three-component seismograms observed by borehole instruments at eleven stations of the KiK-net [*Aoi et al.*, 2000] in order to avoid site effects due to shallow soil conditions. These KiK-net stations are plotted with reverse triangles in Figure 1. The observed accelerograms were numerically integrated to obtain velocity waveforms. The resultant velocities were filtered out with a pass band of 0.02 – 0.5 Hz, and re-sampled with an

interval of 0.2 s. We used the reflectivity method of *Kohketsu* [1985] with an extension to buried receivers to calculate the Green's functions for borehole seismograms [*Koketsu et al.*, 2004].

In order to obtain accurate Green's functions, we determined a set of one-dimensionally stratified velocity models adaptive to the stations in advance using an inverse scheme similar to that of *Ichinose et al.* [2003]. The seismograms from a middle-size aftershock (M_{W} 5.0) at 18:57 on October 23 were inverted with fixed point source parameters and layer velocities. The partial derivatives were numerically calculated by taking the differences between the synthetic seismograms for the initial model and those generated with 5% perturbations of a layer thickness. We then determined the layer thicknesses by an iterative non-linear inversion using the point source parameters from the focal solution by F-net of *NIED* (National Research Institute for Earth Science and Disaster Prevention) [2004]. Figure S1 shows examples of the resultant velocity models and comparisons of the observed and synthetic seismograms. The deduced models were also validated by the comparisons for other aftershocks near the mainshock.

The rupture process inversions were carried out with the method developed by *Yoshida et al.* [1996], which is based on the formulation of multiple time window. Since the slip orientation has been known to be reverse faulting [e.g., *NIED*, 2004], the slip vectors are represented by a linear combination of two components in the directions of $90\pm45^{\circ}$. Each component is constrained not to be negative using the non-negative least square algorithm of *Lawson and Hanson* [1974] instead of the penalty functions in *Yoshida et al.* [1996]. The smoothness constraint with the discrete Laplacian in space and time was also imposed and the weight of the constraint was determined by using ABIC [*Akaike*, 1980]. Even though we constructed the set of adaptive 1-D velocity models, they should still include some incompleteness. In order to reduce possible artifacts due to this incompleteness, scalar time shifts were added to the Green's functions, and their values were also determined by the inversion as in *Graves and Wald* [2001].

4. Fault Models and Slip Distributions

As the fault models we adopted the planes in Figure 2 with the orientations derived from the focal solutions by *NIED* [2004] and preliminary inversions of far-field body waves. We also used the epicenters in Figure 2 for the horizontal locations of the initial rupture breaks of the major events, but their depths were slightly shifted to minimize the residuals between the observed and synthetic waveforms. The fault models were divided into 2×2 km^2 subfaults and the slip histories are represented by a combination of ramp functions with a rise time of 1 s. As described in the previous section, it is difficult to identify the fault planes of the events 2 and 3 in the aftershock distribution. Therefore, we performed two rupture process inversions for both of the plane in Figure 2 and its perpendicular, and then chose the one with a better fit.

In consequence, the planes B and C dipping eastward gave better agreement for the events 2 and 3 as shown in Figure S2. These events, therefore, did not occur on the westward dipping fault planes of the mainshock (event 1) or largest aftershock (event 4), but on those perpendicular to

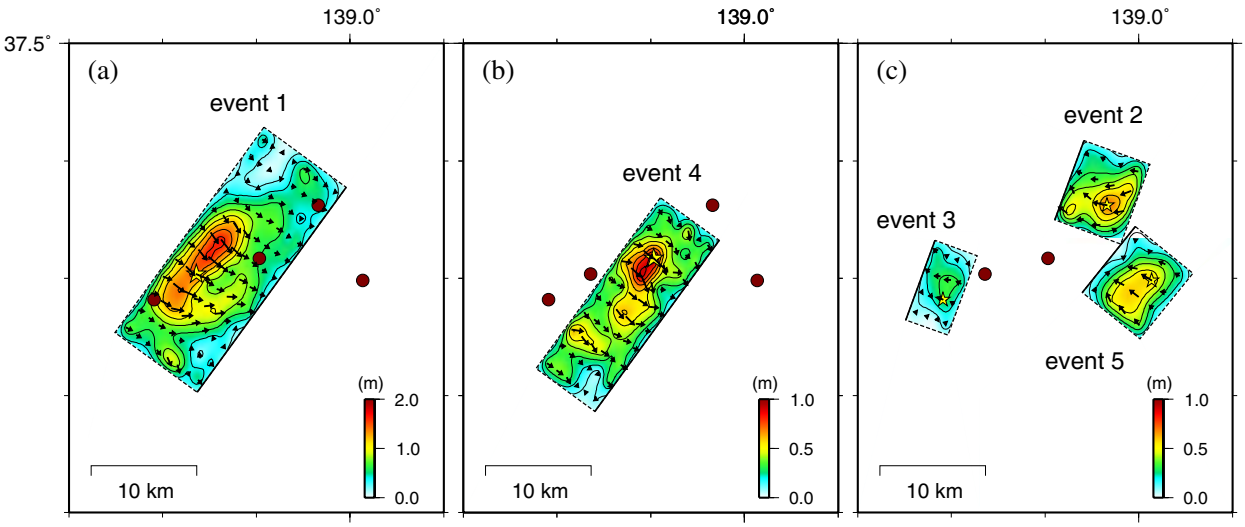

Fig. 3. Surface projections of the recovered slip distributions for (a) the mainshock (event 1), (b) the largest aftershock (event 4) and (c) the other major aftershocks (events 2, 3 and 5). In every fault plane, a yellow star denotes its own rupture break (hypocenter) and brown dots are those of the other events.

them. In other words, the rupture process inversions confirmed that the five major events occurred on five different fault planes. All of the planes extend mostly in the NNE-SSW direction as shown in Figure 3, but two of them dip westward while the others dip eastward. The parameters of these fault planes are summarized in Table 1.

Table 1. Summary of Fault Parameters

No.	Date Time	Strike (°)	Dip (°)	Depth (km)	M_{JMA}	M_{W}	M_{o} (Nm)
1	Oct.23 17:56	216	53	9	6.8	6.6	8.8×10^{18}
2	Oct.23 18:03	20	34	7	6.3	5.9	8.5×10^{17}
3	Oct.23 18:11	20	58	9	6.0	5.7	4.1×10^{17}
4	Oct.23 18:34	216	55	12	6.5	6.3	3.2×10^{18}
5	Oct.27 10:40	39	29	11.5	6.1	5.9	7.5×10^{17}

All the rupture process inversions were carried out with such good performance as found in the waveform comparisons for the mainshock and largest aftershock (Figure S3). Figure 3 also shows the resultant slip distributions projected onto the ground surface. The rupture of the mainshock started from a deep part of the fault plane, and large slips were distributed around the rupture break (hypocenter). Since the maximum slip of about 1.7 m was recovered to the north of the hypocenter and few kilometers away from it (Figure 3a), the rupture mainly propagated northward. The asperity (zone of large slips) of the largest aftershock is also recovered around its hypocenter with the maximum slip of about 1.0m, though the rupture propagated to the south and the slip distribution is more complex than that of the mainshock (Figure 3b). The other events shows simple slip distributions. Each of them looks consisting of a single asperity around the

hypocenter (Figure 3c).

From the recovered slip distributions we calculated static Coulomb failure stress change (ΔCFF) due to the major events. We used the formula of *Okada* [1992] with an apparent frictional coefficient of 0.4 assuming the fault system to be buried in a homogeneous halfspace. Figure 4 shows the distribution of ΔCFF due to the events 1, 2 and 3 immediately before the largest aftershock (event 4). The ΔCFF is positive around the hypocenter and asperity of the largest aftershock. Positive ΔCFFs of 0.03 – 0.28 MPa were also obtained around the hypocenters of the other major aftershocks just before them (Figure S4). Since such association of positive ΔCFF with aftershocks has been widely reported [e.g., *Reasenberg and Simpson*, 1992; *Stein*, 1999], the recovered rupture processes, from which the ΔCFFs were calculated, prove to be reasonable.

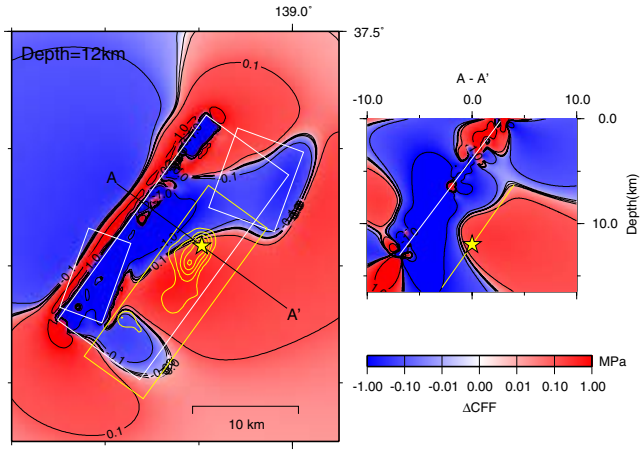

Fig. 4. Distribution of ΔCFF due to the events 1 – 3 (white rectangles) on the horizontal plane at the depth of the hypocenter of the largest aftershock (event 4). The zones of positive ΔCFF are painted in red. The hypocenter, fault plane and asperity of 0.5 m or larger slip are denoted by the yellow star, rectangle and contours, respectively. The right figure is a cross-section along the A-A' line.

5. Conclusions and Discussion

We determined the fault geometry and rupture processes for the five major events of the 2004 Chuetsu earthquake sequence using the strong motion records, hypocenters relocated by the DD method and well calibrated one-dimensionally stratified velocity models. As the result, we recovered the detailed slip distributions and found this earthquake sequence to be a quintuple shock in the complex fault system, where the major events occurred on the five different fault planes. We then calculated the distributions of ΔCFF immediately before the major aftershocks, and found that they were affected by stress change caused by prior events. There should exist many weak planes in the complex geological structure in this source region as a result of past tectonic activities [*Sato*, 1994]. High strain rate has also been observed there [*Sagiya et al.*, 2000]. The mainshock (event 1) occurred because of these tectonic settings. It then acted as a trigger of

the large aftershocks by changing the stress distribution. The large aftershocks also affected the occurrence of following major events in sequence.

The 2004 Chuetsu earthquake sequence is characterized by vital aftershock activities with many large events. The catalog of *JMA* [2005] reports that 88 aftershocks with magnitudes of 4 or greater occurred within a week after the mainshock. The recent crustal earthquakes in Japan, namely, the 1995 Kobe earthquake (M_{W} 6.9) and the 2000 western Tottori earthquake (M_{W} 6.7) reckoned only 46 and 27 $M4$ or greater aftershocks, respectively. We have indicated that there existed at least five notable fault planes and the slips on these faults fitfully occurred in the week. The fault planes are distributed separately as shown in Figure 2, so that the overlap of zones of stress increase is minimized. This resulted in a larger area of aftershock enhancement than that of a usual fault system. Accordingly, aftershocks with greater magnitudes occurred on the separated fault planes. These aftershocks then generated clusters of their own aftershocks.

Acknowledgments

We thank NIED for the strong motion records from KiK-net and the mechanism solutions from F-net. We are also grateful to JMA et al. for the hypocenter list and arrival time data. We appreciate Drs. Waldhauser, Wessel and Smith for the hypoDD and GMT codes. Drs. Shin'ichi Sakai and Aitaro Kato kindly gave us valuable suggestions and discussions. This study was supported by the Special Project for Earthquake Disaster Mitigation in Urban Areas and the Grant-in-Aid for Scientific Research No. 16800054 from the Ministry of Education, Culture, Sports, Science and Technology of Japan.

References

Akaike, H. (1980), Likelihood and Bayes procedure, in *Bayesian Statistics*, edited by J. M. Bernardo *et al.*, pp. 143-166, Univ. Press, Valencia, Spain.

Aoi, S., K. Obara, S. Hori, K. Kasahara, and Y. Okada (2000), New strong-motion observation network: KiK-net, *Eos Trans. AGU*, *81 (48)*,Fall Meet. Suppl., Abstract S71A-05.

FDMA (2005), *The 2004 Chuetsu, Niigata, earthquake (No. 66)*, http://www.fdma.go.jp/data/010502221022317478.pdf.

Graves, R. W., and D. J. Wald (2001), Resolution analysis of finite fault source inversion using one- and three-dimensional Green's functions 1. Strong motions, *J. Geophys. Res.*, *106*, 8745-8766.

Ichinose, G. A., H. K. Thio, P. G. Somerville, T. Sato, and T. Ishii (2003), Rupture process of the 1994 Tonankai earthquake (M_{S}8.1) from the inversion of teleseismic and regional seismograms, *J. Geophys. Res.*, *108*, doi:10.1029/2003JB002393.

JMA (2005), *The Seismological and Volcanological Bulletin of Japan for October 2004*, JMA, Tokyo.

Kato, A., E. Kurashimo, N. Hirata, S. Sakai, T. Iwasaki, and T. Kanazawa (2005), Imaging the source region of the 2004 mid-Niigata prefecture earthquake and the evolution of a seismogenic thrust-related fold, *Geophys. Res. Lett.*, *32*, doi:10.1029/2005GL022366, in press.

Kohketsu, K. (1985), The extended reflectivity method for synthetic near-field seismograms, *J. Phys. Earth*, *33*, 121–131.

Koketsu, K., K. Hikima, S. Miyazaki and S. Ide (2004), Joint inversion of strong motion and geodetic data for the source process of the 2003 Tokachi-oki, Hokkaido, earthquake, *Earth Planets Space*, *56*, 329–334.

Lawson, C. L., and R. J. Hanson (1974), Solving Least Squares Problems, Prentice-Hall, Englewood Cliffs., N. J.

NIED (2004), *Earthquake Mechanism Information*, http://www.fnet.bosai.go.jp/freesia/event/hypo/joho.htm

Okada, Y. (1992), Internal deformation due to shear and tensile faults in a half-space, *Bull. Seismol. Soc. Am.*, *82*, 1018-1040.

Page, R. (1968), Aftershock and microaftershocks of the great Alaska earthquake of 1964, *Bull. Seismol. Soc. Am.*, *58*, 1131–1168.

Reasenberg, P. A., and R. W. Simpson (1992), Response of regional seismicity to the static stress change produced by the Loma Prieta earthquake, *Science*, *255*, 1687-1690.

Sagiya, T., S. Miyazaki, and T. Tada (2000), Continuous GPS array and present-day crustal deformation of Japan, *Pure Appl. Geophys.*, *38*, 2303-2322.

Sato, H. (1994), The relationship between late Cenozoic tectonic events and stress field and basin development in northeast Japan, *J. Geophys. Res.*, *99*, 22261-22274.

Sidle, R. C., T. Kamai, and A. C. Trandafir (2005), Evaluating landslide damage during the 2004 Chuetsu earthquake, Niigata, Japan, *EOS Trans. AGU*, *86(13)*, 133–136.

Stein, R. S. (1999), The role of stress transfer in earthquake occurrence, *Nature*, *402*, 605-609.

Yoshida, S., K. Koketsu, B. Shibazaki, T. Sagiya, T. Kato, and Y. Yoshida (1996), Joint inversion of near- and far- field waveforms and geodetic data for the rupture process of the 1995 Kobe earthquake, *J. Phys. Earth*, *44*, 437–454.

Waldhauser, F., and W. L. Ellsworth (2000), A double-difference earthquake location algorithm: method and application to the Northern Hayward fault, California, *Bull. Seismol. Soc. Am.*, *90*, 1353-1368.

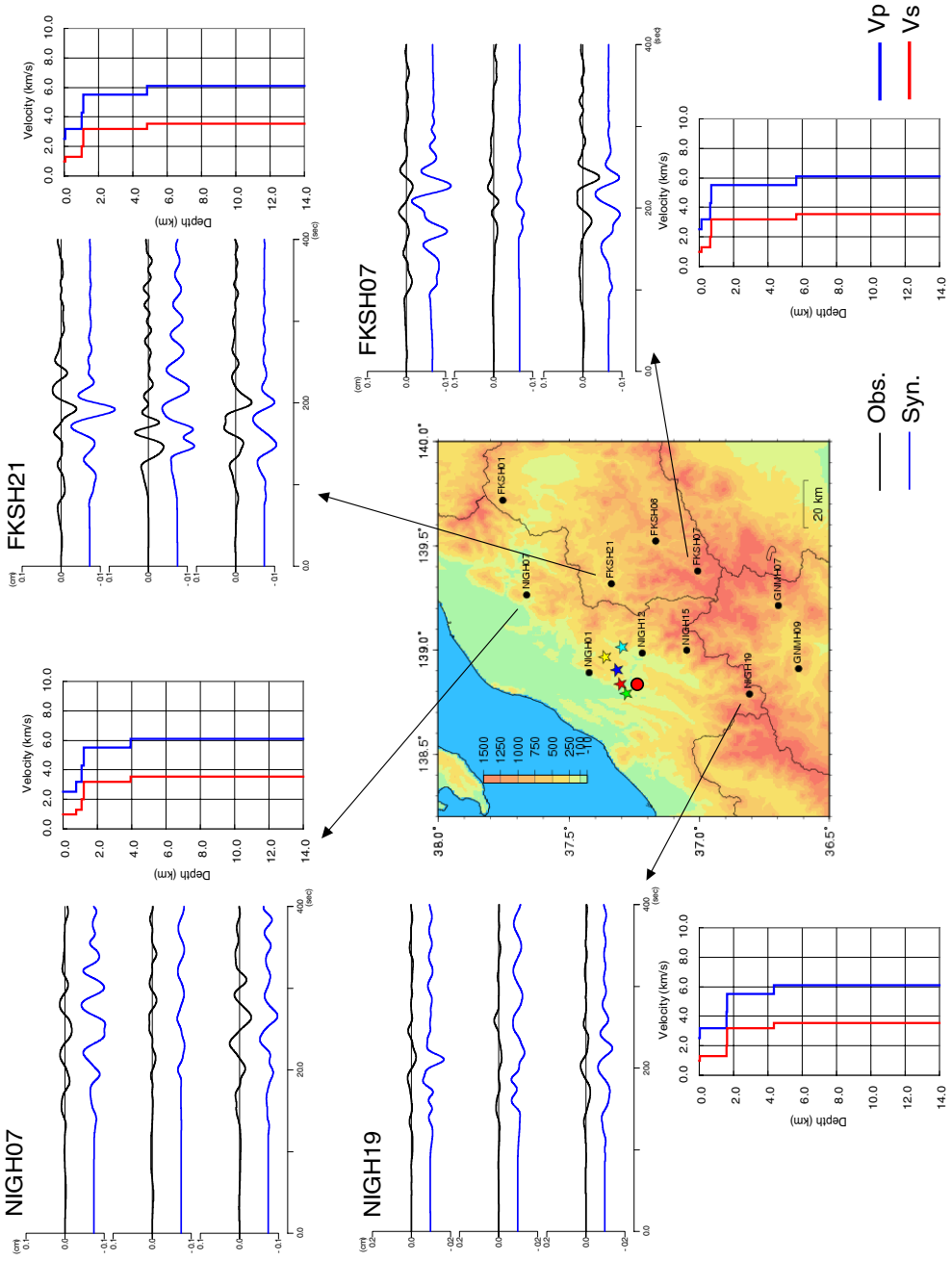
FKSH21
FKSH07
NIGH07
NIGH19
Obs.
Syn.
Vp
Vs
Velocity (km/s)
Depth (km)
20 km
FKSH01
FKSH06
FKSH07
FKSH21
NIGH01
NIGH07
NIGH12
NIGH15
NIGH19
GNMH07
GNMH09
1500
1250
1000
750
500
250
100
140.0°
139.5°
139.0°
138.5°
38.0°
37.5°
37.0°
36.5°

Figure S1

(a)

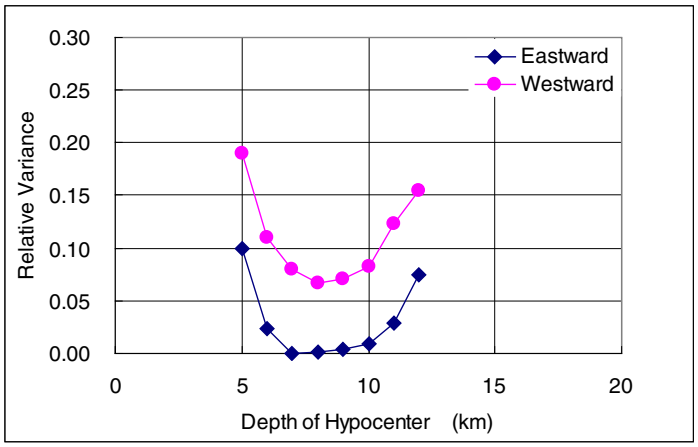

(b)

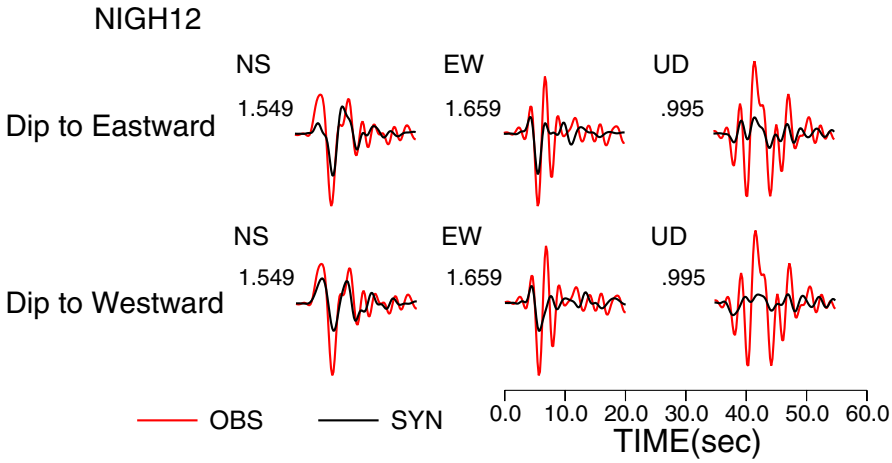

Figure S2(a)

(a)

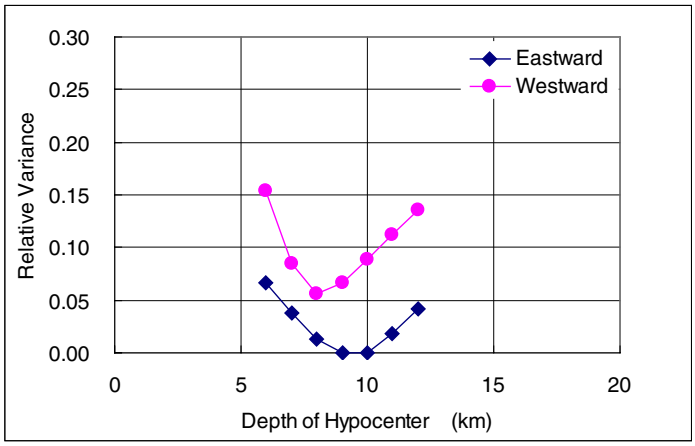

(b)

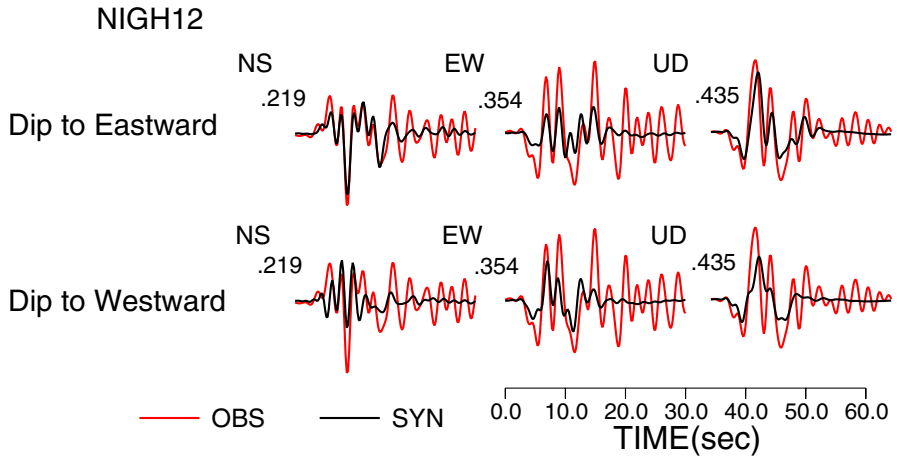

Figure S2(b)

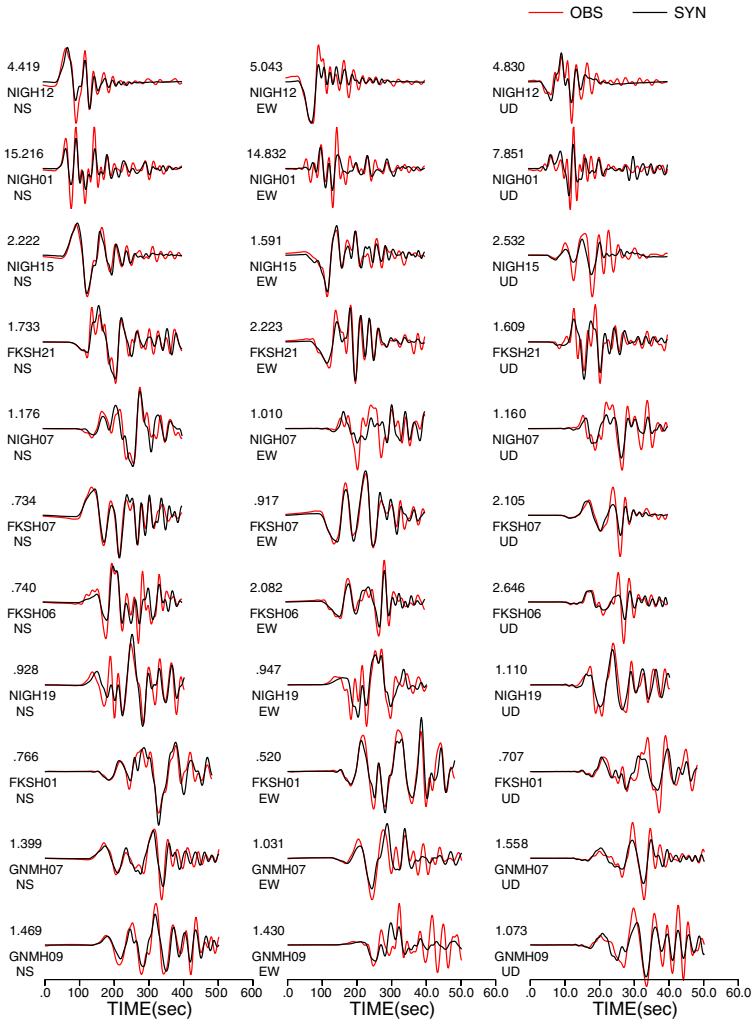
OBS
SYN
4.419
NIGH12
NS
15.216
NIGH01
NS
2.222
NIGH15
NS
1.733
FKSH21
NS
1.176
NIGH07
NS
.734
FKSH07
NS
.740
FKSH06
NS
.928
NIGH19
NS
.766
FKSH01
NS
1.399
GNMH07
NS
1.469
GNMH09
NS
5.043
NIGH12
EW
14.832
NIGH01
EW
1.591
NIGH15
EW
2.223
FKSH21
EW
1.010
NIGH07
EW
.917
FKSH07
EW
2.082
FKSH06
EW
.947
NIGH19
EW
.520
FKSH01
EW
1.031
GNMH07
EW
1.430
GNMH09
EW
4.830
NIGH12
UD
7.851
NIGH01
UD
2.532
NIGH15
UD
1.609
FKSH21
UD
1.160
NIGH07
UD
2.105
FKSH07
UD
2.646
FKSH06
UD
1.110
NIGH19
UD
.707
FKSH01
UD
1.558
GNMH07
UD
1.073
GNMH09
UD
.0 100 200 300 400 500 600
TIME(sec)
.0 100 200 300 40.0 50.0 60.0
TIME(sec)
.0 10.0 20.0 30.0 40.0 50.0 60.0
TIME(sec)

Figure S3(a)

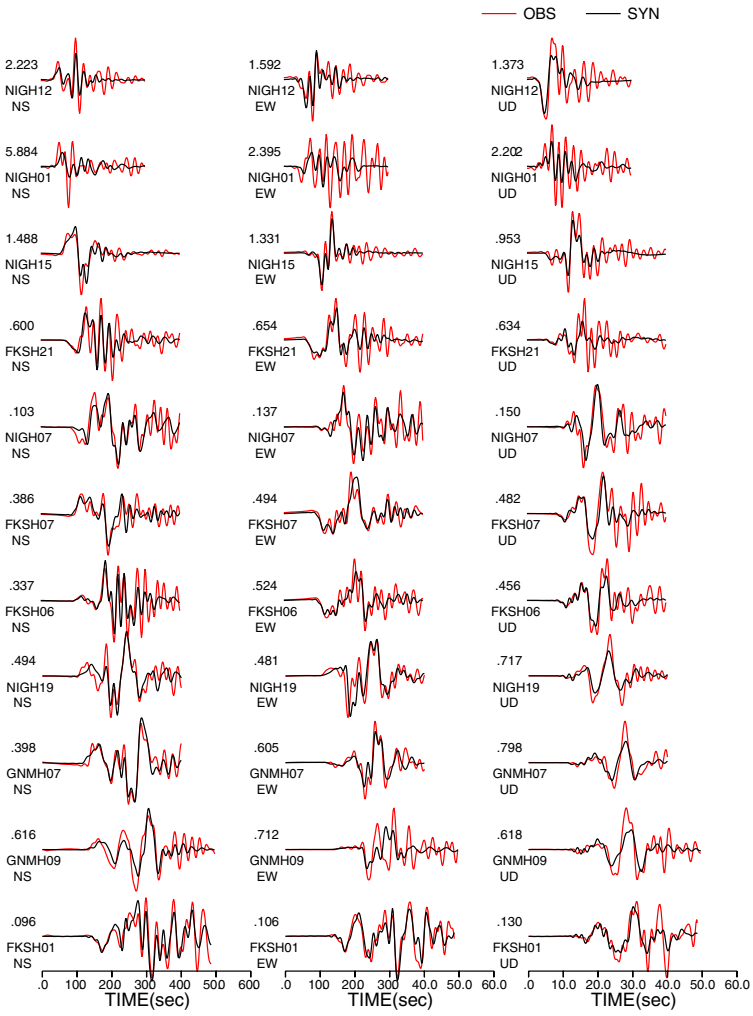
OBS
SYN
2.223
NIGH12
NS
5.884
NIGH01
NS
1.488
NIGH15
NS
.600
FKSH21
NS
.103
NIGH07
NS
.386
FKSH07
NS
.337
FKSH06
NS
.494
NIGH19
NS
.398
GNMH07
NS
.616
GNMH09
NS
.096
FKSH01
NS
1.592
NIGH12
EW
2.395
NIGH01
EW
1.331
NIGH15
EW
.654
FKSH21
EW
.137
NIGH07
EW
.494
FKSH07
EW
.524
FKSH06
EW
.481
NIGH19
EW
.605
GNMH07
EW
.712
GNMH09
EW
.106
FKSH01
EW
1.373
NIGH12
UD
2.202
NIGH01
UD
.953
NIGH15
UD
.634
FKSH21
UD
.150
NIGH07
UD
.482
FKSH07
UD
.456
FKSH06
UD
.717
NIGH19
UD
.798
GNMH07
UD
.618
GNMH09
UD
.130
FKSH01
UD
.0 100 200 300 400 500 600
TIME(sec)
.0 100 200 300 40.0 50.0 60.0
TIME(sec)
.0 10.0 20.0 30.0 40.0 50.0 60.0
TIME(sec)

Figure S3(b)

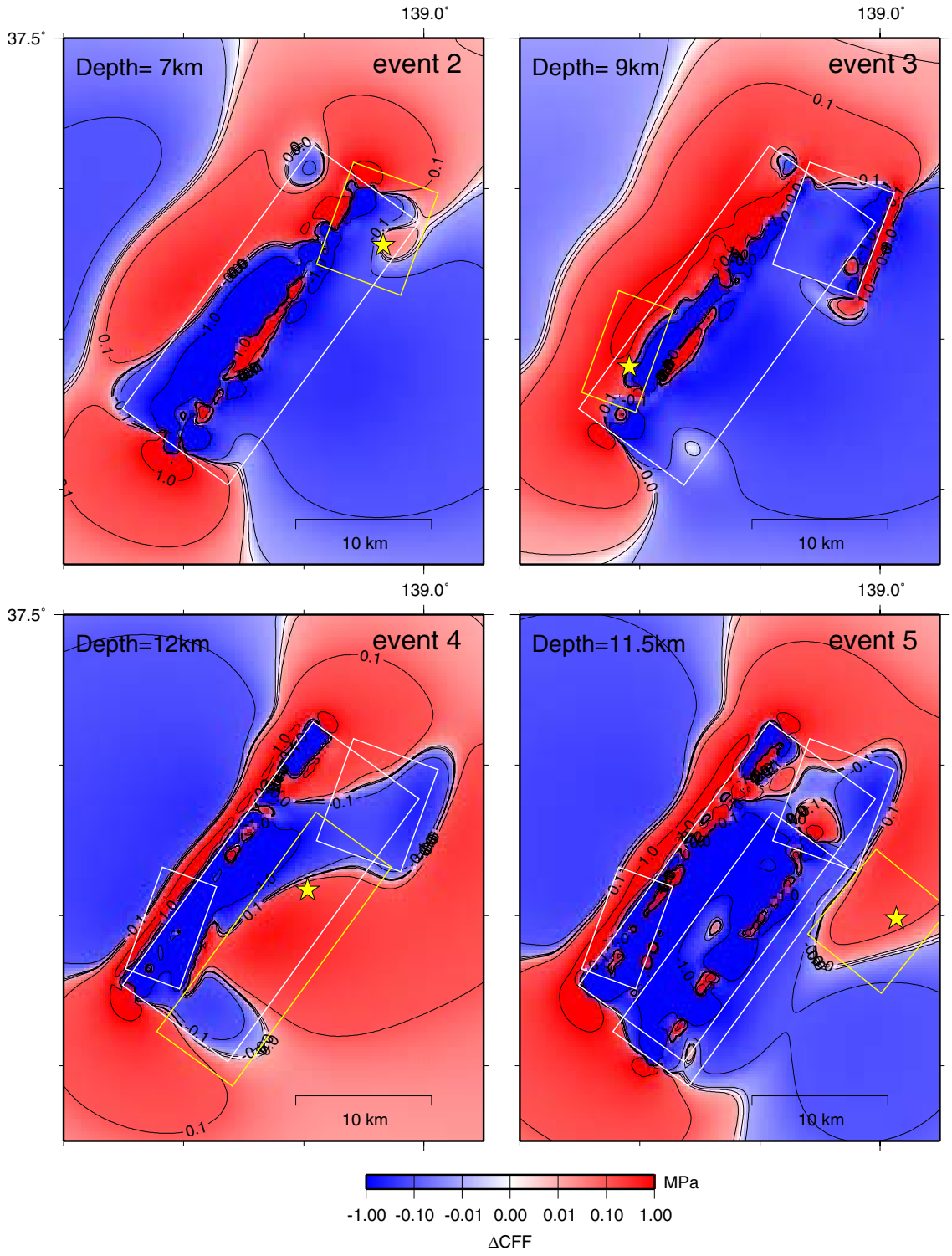
139.0˚
37.5˚
Depth= 7km
event 2
Depth= 9km
event 3
Depth=12km
event 4
Depth=11.5km
event 5
10 km
MPa
-1.00 -0.10 -0.01 0.00 0.01 0.10 1.00
ΔCFF

Figure S4